RESEARCH OF THE AEROPHYSICS INSTITUTE FOR THE STRATEGIC TECHNOLOGY OFFICE (DARPA)

POLYTECHNIC INSTITUTE OF NEW YORK
FARMINGDALE

30 JUNE 1975

RESEARCH OF THE AEROPHYSICS INSTITUTE FOR THE STRATEGIC TECHNOLOGY OFFICE (DARPA)

by

MARTIN H. BLOOM

1 JULY 1974 THROUGH 30 JUNE 1975

OFFICE OF NAVAL RESEARCH

CONTRACT NO. N00014-67-A-0438-0017

POLYTECHNIC INSTITUTE OF NEW YORK

Sponsored by

Advanced Research Projects Agency

ARPA ORDER NO. 2684

The views and conclusions contained in this document are those of the authors and should not be interpreted as necessarily representing the official policies, either expressed or implied, of the Advanced Research Projects Agency or the U. S. Government.

SECURITY CLASSIFICATION OF THIS PAGE (When Data Entered)

REPORT DOCUMENTATION PAGE

READ INSTRUCTIONS BEFORE COMPLETING FORM

1. REPORT NUMBER
2. GOVT ACCESSION NO.
3. RECIPIENT'S CATALOG NUMBER

4. TITLE (and Subtitle)
RESEARCH OF THE AEROPHYSICS INSTITUTE FOR THE STRATEGIC TECHNOLOGY OFFICE (DARPA)

5. TYPE OF REPORT & PERIOD COVERED
Final Technical Report
1 July 1974 - 30 June 1975

6. PERFORMING ORG. REPORT NUMBER

7. AUTHOR(s)
M. H. BLOOM

8. CONTRACT OR GRANT NUMBER(s)
N00014-67-A-0438-0017

9. PERFORMING ORGANIZATION NAME AND ADDRESS
Polytechnic Institute of New York
Route 110
Farmingdale, N. Y. 11735

10. PROGRAM ELEMENT, PROJECT, TASK AREA & WORK UNIT NUMBERS
ARPA Order No. 2684

11. CONTROLLING OFFICE NAME AND ADDRESS
Advanced Research Projects Agency
1400 Wilson Blvd.
Arlington, Va. 22209

12. REPORT DATE

13. NUMBER OF PAGES
40

14. MONITORING AGENCY NAME & ADDRESS(if different from Controlling Office)
Office of Naval Research
Dept. of the Navy
Arlington, Va 22217

15. SECURITY CLASS. (of this report)
Unclassified

15a. DECLASSIFICATION/DOWNGRADING SCHEDULE

16. DISTRIBUTION STATEMENT (of this Report)
Approved for public release;
Distribution unlimited.

17. DISTRIBUTION STATEMENT (of the abstract entered in Block 20, if different from Report)

18. SUPPLEMENTARY NOTES
→ Research was continued on

19. KEY WORDS (Continue on reverse side if necessary and identify by block number)
1. Image Recovery & Processing
2. Finite-Sized Object
3. Deconvolution & Apodization
4. Band-Limited Function
5. Discrete Fourier Series & Fast Fourier Transform

(continued on reverse side)

20. ABSTRACT (Continue on reverse side if necessary and identify by block number)

The Polytechnic's DARPA-STO-Aerophysics Institute program during the subject period was centered on the improvement of long-range image recognition, i.e., optical discrimination, and on the study of certain laser pnenomena.

In the optics area, it was desired to improve the image recovery of an object of finite size from its diffraction-limited image in order to enhance the remote observation of high-altitude objects, such as satellites, perceived through the fluctuating atmosphere. A new algorithm is proposed for comting the transfer of a band-limited function.

(continued on reverse side)

DD FORM 1 JAN 73 1473 EDITION OF 1 NOV 65 IS OBSOLETE

Unclassified
SECURITY CLASSIFICATION OF THIS PAGE (When Data Entered)

19. (continued)

6. Unstable Optical Resonator Cavities
7. Laser Metal Screening Program
8. Ultraviolet & Blue-Green Lasers
9. Efficient Metal-Vapor Lasers
10. Atomic Transition Probabilities
11. Computer Modeling of Laser Dynamic
12. Startified Ocean Wakes

20. (continued)

In the laser area, the major task was the screening of atomic vapors, particularly metal vapors, for new, efficient lasers in the visible and ultraviolet spectral ranges, using computer-modeling and experimental methods. Several promising candidates are identified. In another vein, the theory of unstable resonator cavities was studied in relation to lasers, with a view toward improving the analytic methodology as a complement to numerical techniques, and toward improving design by improving the understanding of the resonance phenomena in cavity configurations.

The developments in these areas are summarized herein.

A minor effort in this program period was devoted to completion of the final reportage on the experimental simulation of stratified ocean wakes in our thermally-stratified air wind-tunnel. The actual work had been completed in the prior program period.

POLYTECHNIC INSTITUTE OF NEW YORK
DARPA-STO AEROPHYSICS INSTITUTE PROGRAM
July 1, 1974 - June 30, 1975

INTRODUCTION

The Polytechnic's DARPA-STO-Aerophysics Institute program during the subject period was centered on the improvement of long-range image recognition, i.e., optical discrimination, and on the study of certain laser pnenomena.

In the optics area, it was desired to improve the image recovery of an object of finite size from its diffraction-limited image in order to enhance the remote observation of high-altitude objects, such as satellites, perceived through the fluctuating atmosphere. A new algorithm is proposed for computing the transfer of a band-limited function.

In the laser area, the major task was the screening of atomic vapors, particularly metal vapors, for new, efficient lasers in the visible and ultraviolet spectral ranges, using computer-modeling and experimental methods. Several promising candidates are identified. In another vein, the theory of unstable resonator cavities was studied in relation to lasers, with a view toward improving the analytic methodology as a complement to numerical techniques, and toward improving design by improving the understanding of the resonance phenomena in cavity configurations.

The developments in these areas are summarized herein.

A minor effort in this program period was devoted to completion of the final reportage on the experimental simulation of stratified ocean wakes in our thermally-stratified air wind-tunnel (see Appendix III). The actual work had been completed in the prior program period.

The principal participants in the program were Profs. A. Papoulis and L. Felsen (currently Dean of Engineering), and Dr. William Walter. Prof. M.H. Bloom served as coordinator of the program.

IMAGE-RECOVERY OF AN OBJECT OF FINITE SIZE FROM ITS DIFFRACTION-LIMITED IMAGE

A. Papoulis

Under the usual assumptions, the image $q(x, y)$ of an object $p(x, y)$ can be expressed as a convolution

$$q(x, y) = \int_{-\infty}^{\infty} \int_{-\infty}^{\infty} p(x-\xi, y-\eta)\, h(\xi, \eta)\, d\xi\, d\eta$$

In the coherent case, $p(x, y)$ and $q(x, y)$ are amplitudes and $h(x, y)$ is the point spread of the system. In the incoherent case, $p(x, y)$ and $q(x, y)$ are intensities (illuminance functions) and $h(x, y)$ is the square of the point spread.

Due to the diffraction effect, the transform modulation transfer function

$$H(u, v) = \int_{-\infty}^{\infty} \int_{-\infty}^{\infty} h(x, y)\, e^{-j(ux+vy)}\, dx\, dy$$

is space limited:

$$H(u, v) = 0 \quad \text{for} \quad u^2 + v^2 > a^2$$

resulting in a distortion of the object $p(x, y)$.

An important problem in image processing is the reduction of this distortion (deconvolution). Known methods involve the introduction of an optical filter on the aperture plane (apodization). In these methods the high frequency components of the object are lost.

In this work, a method is developed for the recovery of $p(x, y)$ under the assumption that the object is of finite size. The recovery, in principle, of $p(x, y)$ is a consequence of the analytic properties of its transform $P(u, v)$. However, known techniques of analytic continuation are not practical.

The approach proposed here is based on a simple efficient algorithm involving only discrete Fourier series and Fast Fourier transforms. The algorithm involves an iteration converging to the exact value of the object p(x, y) in the absence of noise. The effects of noise are determined and an early termination of the iteration is suggested for optimum results.

Details of the method for the one-dimensional problem are shown in the attached paper.

IEEE TRANSACTIONS ON CIRCUITS AND SYSTEMS, VOL. CAS-22, NO. 9, SEPTEMBER 1975

A New Algorithm in Spectral Analysis and Band-Limited Extrapolation

ATHANASIOS PAPOULIS, FELLOW, IEEE

Abstract—If only a segment of a function $f(t)$ is given, then its Fourier spectrum $F(\omega)$ is estimated either as the transform of the product of $f(t)$ with a time-limited window $w(t)$, or by certain techniques based on various *a priori* assumptions. In the following, a new algorithm is proposed for computing the transform of a band-limited function. The algorithm is a simple iteration involving only the fast Fourier transform (FFT). The effect of noise and the error due to aliasing are determined and it is shown that they can be controlled by early termination of the iteration.

The proposed method can also be used to extrapolate band-limited functions.

I. Introduction

A CENTRAL PROBLEM in Fourier analysis and spectral estimation is the determination of the transform

$$F(\omega) = \int_{-\infty}^{\infty} f(t)e^{-j\omega t}\,dt \tag{1}$$

of a signal $f(t)$ in terms of a finite segment

$$g(t) = f(t)p_T(t), \qquad p_T(t) = \begin{cases} 1, & |t| < T \\ 0, & |t| > T \end{cases} \tag{2}$$

of $f(t)$. The known estimation methods can be separated into the following two classes.

1) (See Blackman–Tukey [1].) The available segment $g(t)$ is multiplied by a "window" $w(t)$ and the integral

$$F_w(\omega) = \int_{-T}^{T} w(t)f(t)e^{-j\omega t}\,dt = \frac{1}{2\pi}\int_{-\infty}^{\infty} F(\omega - y)W(y)\,dy \tag{3}$$

is used as the estimator of $F(\omega)$. The pair $w(t) \leftrightarrow W(\omega)$ is so chosen as to minimize in some sense the resulting error $F_w(\omega) - F(\omega)$ [2], [3]. In this approach, the inverse transform $f(t)w(t)$ of the estimator $F_w(\omega)$ is zero for $|t| > T$.

2) The unknown part of $f(t)$ is not assumed to be zero as in 1) but it is determined by some form of extrapolation. This is possible only if various *a priori* assumptions about for form of $F(\omega)$ are made.

Manuscript received November 15, 1974; revised March 26, 1975. This work was supported in part by the Joint Services Electronics Program under Contract F44620-69-C-0047 and in part by the Advanced Research Projects Agency of the Department of Defense, and was monitored by the Office of Naval Research under Contract N00014-67-A-0438-0017.

The author is with the Polytechnic Institute of New York, Farmingdale, N.Y. 11735.

Class 2) includes the method of maximum entropy [4] (see Appendix A) and the techniques for extrapolating band-limited functions.

Band-Limited Functions

We shall say that a function $f(t)$ is band-limited, if its energy E is finite and its transform $F(\omega)$ is zero outside a finite interval

$$F(\omega) = 0, \qquad \text{for } |\omega| > \sigma. \tag{4}$$

A band-limited function is analytic in the entire t-axis [5], hence its Taylor-series expansion yields $f(t)$ for every t. We have thus an extrapolation method (analytic continuation) based on (4), however, as it is well known, we cannot use it for recovering $f(t)$ from real data.

In this paper, we develop a new method for computing $f(t)$ and its transform $F(\omega)$ from the given segment $g(t)$. The method is based on a simple efficient algorithm involving only discrete Fourier series and a fast Fourier transform (FFT). The algorithm is presented in analog form. The numerical implementation is carried out digitally but, since the analog to digital conversion is well known, the details are omitted.

We note that the proposed algorithm (Section II) has been used by Gerchberg in a recent paper on picture processing [6].

Another method of extrapolating band-limited functions is based on the expansion of $g(t)$ into a series of prolate spheroidal functions [7]. This method is compared with ours in Section V.

II. An Iteration Method for Computing the Fourier Transform of a Band-Limited Function

We wish to determine the Fourier transform $F(\omega)$ of a band-limited function $f(t)$ (Fig. 1) in terms of the finite segment $g(t)$ of $f(t)$ [see (2)]. The proposed method is an iteration starting with the transform

$$G(\omega) = G_0(\omega) = \int_{-T}^{T} g(t)e^{-j\omega t}\,dt$$

of the given segment $g(t) = g_0(t)$. The nth iteration step proceeds as follows.

We form the function

$$F_n(\omega) = G_{n-1}(\omega)p_\sigma(\omega), \qquad p_\sigma(\omega) = \begin{cases} 1, & |\omega| < \sigma \\ 0, & |\omega| > \sigma \end{cases} \tag{5}$$

 Annals No. 509CA004

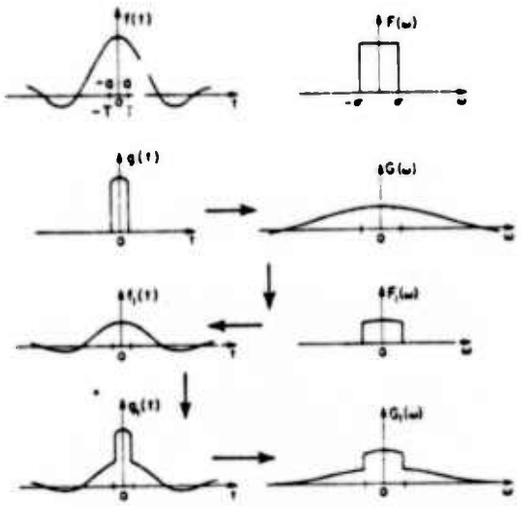

Fig. 1. Unknown pair $f(t) \leftrightarrow F(\omega)$ and signals of first iteration.

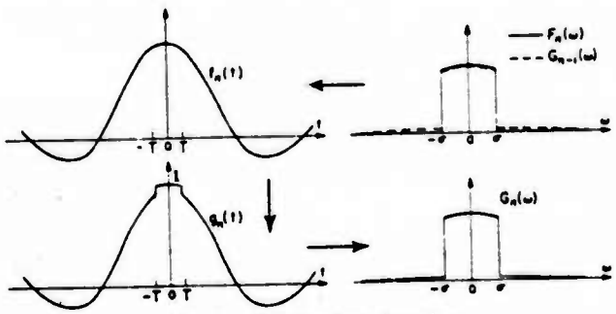

Fig. 2. Signals of nth iteration.

obtained by truncating $G_{n-1}(\omega)$ as in Fig. 2, and compute its inverse transform

$$f_n(t) = \int_{-\sigma}^{\sigma} F_n(\omega)e^{j\omega t}\,d\omega. \tag{6}$$

We, next, form the function

$$g_n(t) = f_n(t) + [f(t) - f_n(t)]p_T(t) = \begin{cases} g(t), & |t| < T \\ f_n(t), & |t| > T \end{cases} \tag{7}$$

obtained by replacing the segment of $f_n(t)$ in the interval $(-T,T)$ by the known segment $g(t)$ of $f(t)$. The nth step ends by computing the transform

$$G_n(\omega) = \int_{-\infty}^{\infty} g_n(t)e^{-j\omega t}\,dt \tag{8}$$

of the function $g_n(t)$ so formed.

We note that the function $f_n(t)$ is band-limited and it is given by

$$f_n(t) = g_{n-1}(t) * \frac{\sin \sigma t}{\pi t}. \tag{9}$$

This follows from (5) and the convolution theorem [8]. From (9) we conclude that $f_n(t)$ can be obtained as the output of an ideal low-pass filter with input $g_{n-1}(t)$. A two-input gate at the output of the filter, switching from $f_n(t)$ to

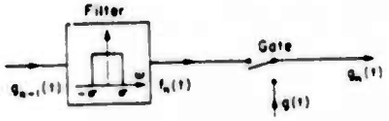

Fig. 3. Analog simulation of iteration.

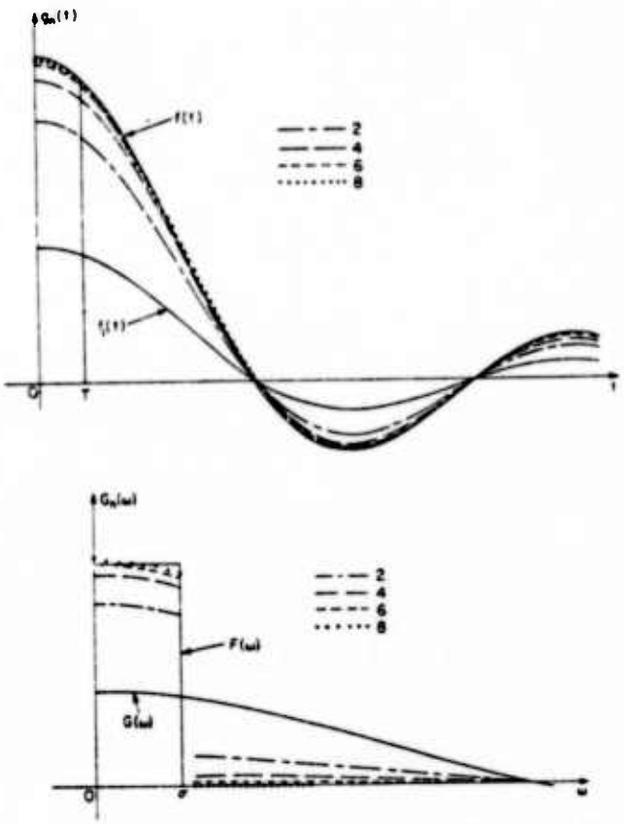

Fig. 4. Computer output of $g_n(t)$ and $G_n(\omega)$ for $f(t) = \sin \sigma t/\pi t$ and $n = 2, 4, 6$, and 8.

the given segment $g(t)$ of $f(t)$ as in (7), yields $g_n(t)$ (Fig. 3).

It will be shown in the next section that the functions $f_n(t)$ and $F_n(\omega)$ tend to $f(t)$ and $F(\omega)$, respectively, as $n \to \infty$. The iteration is thus a method for computing $F(\omega)$ and for extrapolating a band-limited function $f(t)$.

Numerical Illustration

We have applied the method to the pair

$$f(t) = \frac{\sin \sigma t}{\pi t} \leftrightarrow F(\omega) = p_\sigma(\omega)$$

choosing for T the value $\pi/5\sigma$. The numerical results are shown in Fig. 4 for $n = 2,4,6,8$. As we see from the figure, although the data interval is only 1/5 of the main lobe of $f(t)$, the convergence of $F_n(\omega)$ to the unknown spectrum $p_\sigma(\omega)$ is remarkably rapid. With this T, the method of windows would yield no satisfactory estimate of $F(\omega)$. We should point out, however, that the speed of convergence observed for this example is due to the fact that in the expansion (11) of the function $\sin \sigma t/\pi t$, only the first few terms are significant. As we show in Section IV, if this is not the case, the convergence is slow.

Mean-Square Error Reduction

From (5), (7), and Parseval formula [8] it follows that

$$\frac{1}{2\pi}\int_{-\infty}^{\infty} |F(\omega) - G_{n-1}(\omega)|^2\, d\omega$$

$$> \frac{1}{2\pi}\int_{-\sigma}^{\sigma} |F(\omega) - F_n(\omega)|^2\, d\omega$$

$$= \int_{-\infty}^{\infty} |f(t) - f_n(t)|^2\, dt > \int_{-\infty}^{\infty} |f(t) - g_n(t)|^2\, dt$$

$$= \frac{1}{2\pi}\int_{-\infty}^{\infty} |F(\omega) - G_n(\omega)|^2\, d\omega. \tag{10}$$

Thus the use of the available information about $f(t)$ (band-limited for $|\omega| > \sigma$ and known for $|t| < T$) results in a reduction of the mean-square error twice at each iteration step.

III. Convergence

To prove the convergence of the iteration, we expand the band-limited function $f(t)$ into a series

$$f(t) = \sum_{k=0}^{\infty} a_k \phi_k(t) \tag{11}$$

where $\phi_k(t)$ are the prolate spheroidal wave functions [see (68)].

Theorem 1

The function $f_n(t)$ of the nth iteration is given by

$$f_n(t) = f(t) - \sum_{k=0}^{\infty} a_k(1 - \lambda_k)^n \phi_k(t) \tag{12}$$

where λ_k are the eigenvalues of (63) corresponding to the eigenfunctions $\phi_k(t)$.

Proof: Suppose, first, that

$$f(t) = \phi_k(t).$$

We shall show by induction that

$$f_n(t) = A_n \phi_k(t), \qquad \text{where } A_n = 1 - (1 - \lambda_k)^n. \tag{13}$$

Indeed, (13) is true for $n = 1$. Suppose that it is true for some $n \geq 1$. It, then, follows from (7), (9), and (63) that

$$g_n(t) = A_n \phi_k(t) + (1 - A_n)\phi_k(t) p_T(t). \tag{14}$$

Inserting into (9) and using (63) and (67), we obtain

$$f_{n+1}(t) = A_n \phi_k(t) + (1 - A_n)\lambda_k \phi_k(t) \tag{15}$$

hence,

$$f_{n+1}(t) = A_{n+1}\phi_k(t)$$

where

$$A_{n+1} = A_n + (1 - A_n)\lambda_k, \qquad n \geq 1. \tag{16}$$

Solving the recursion equation (16) with the initial condition $A_1 = \lambda_k$, we obtain (13).

Applying (13) to each term in (11), we conclude that

$$f_n(t) = \sum_{k=0}^{\infty} a_k[1 - (1 - \lambda_k)^n]\phi_k(t) \tag{17}$$

and (12) results.

Theorem 2

For any t,

$$f_n(t) \to f(t) \quad \text{as} \quad n \to \infty. \tag{18}$$

Proof: As we see from (12), the error

$$e_n(t) = f(t) - f_n(t) \tag{19}$$

is given by

$$e_n(t) = \sum_{k=0}^{\infty} a_k(1 - \lambda_k)^n \phi_k(t) \tag{20}$$

and its mean-square value E_n by

$$E_n = \int_{-\infty}^{\infty} e_n^2(t)\, dt = \sum_{k=0}^{\infty} a_k^2(1 - \lambda_k)^{2n} \tag{21}$$

[see (70)]. We maintain that

$$E_n \to 0 \quad \text{with} \quad n \to \infty. \tag{22}$$

Indeed, the energy

$$E = \sum_{k=0}^{\infty} a_k^2 \tag{23}$$

of $f(t)$ is finite by assumption; hence, given $\varepsilon > 0$, we can find an integer N such that

$$\sum_{k>N} a_k^2 < \varepsilon.$$

The eigenvalues λ_k are less than 1 and tend to zero monotonically as $k \to \infty$. Therefore, $1 - \lambda_k < 1$ and

$$1 - \lambda_k \leq 1 - \lambda_N, \qquad \text{for } k \leq N.$$

From the above we conclude that

$$E_n = \sum_{k=0}^{N} + \sum_{k>N} a_k^2(1 - \lambda_k)^{2n}$$

$$< (1 - \lambda_N)^{2n} \sum_{k=0}^{N} a_k^2 + \sum_{k>N} a_k^2 < (1 - \lambda_N)^{2n} E + \varepsilon$$

and (22) results because ε is arbitrary and

$$(1 - \lambda_N)^{2n} \to 0 \quad \text{with} \quad n \to \infty.$$

To complete the proof of the theorem, we observe that

$$|e_n(t)| \leq \sqrt{\frac{E_n \sigma}{\pi}}. \tag{24}$$

This follows from the fact that the transform of $e_n(t)$ is zero for $|\omega| > \sigma$ [9]. Thus $e_n(t) \to 0$ with $n \to \infty$ and (18) results.

We note for later use that [see (7), (12), and (66)]

$$G(\omega) = B \sum_{k=0}^{\infty} a_k \sqrt{\lambda_k}\, \phi_k(b\omega), \qquad B = \sqrt{\frac{2\pi T}{\sigma}}, \qquad b = \frac{T}{\sigma} \tag{25}$$

$$F_n(\omega) = Bp_\sigma(\omega) \sum_{k=0}^{\infty} \frac{a_k}{\sqrt{\lambda_k}} [1 - (1 - \lambda_k)^n] \phi_k(b\omega) \tag{26}$$

$$G_n(\omega) = F_n(\omega) + B \sum_{k=0}^{\infty} a_k \sqrt{\lambda_k} (1 - \lambda_k)^n \phi_k(b\omega). \tag{27}$$

Reasoning similarly, we conclude that the function $F_n(\omega)$ and $G_n(\omega)$ tend to $F(\omega)$ with $n \to \infty$.

IV. Error Analysis

The proposed method is subject to the following errors: truncation of the iteration; aliasing due to high frequencies in $F(\omega)$; noise; computer roundoff; analog to digital conversion. These errors depend on the nature of $f(t)$ and on the product σT. In the following, we examine their effect on the estimate $F_n(\omega)$ of $F(\omega)$. The analog to digital conversion error involving the evaluation of the Fourier integrals by discrete Fourier series is well known and will not be discussed.

Truncation Error

If the iteration is terminated at the nth step and the function $F_n(\omega)$ is used as the estimate of $F(\omega)$, the resulting mean-square error is given by [see (21)]

$$E_n = \frac{1}{2\pi} \int_{-\sigma}^{\sigma} |F(\omega) - F_n(\omega)|^2 \, d\omega = \sum_{k=0}^{\infty} a_k^2 (1 - \lambda_k)^{2n} \tag{28}$$

where λ_k are the eigenvalues of (63). As we see from Fig. 5, the λ_k's increase as the product σT increases and they tend to 1 with $\sigma T \to \infty$ [10]. Thus if σT is large, the required number of iterations is small.

The error E_n depends also on the coefficients a_n. If n is small, then the contribution of the high-order terms in (28) is small. However, as n increases, their effect becomes relatively more significant because the difference $1 - \lambda_k$ tends to 1 with $k \to \infty$.

From (27) it follows after some thought that the energy I_n of $G_n(\omega)$ outside the band $(-\sigma,\sigma)$ is given by

$$I_n = \frac{1}{2\pi} \int_{|\omega|>\sigma} |G_n(\omega)|^2 \, d\omega = \sum_{k=0}^{\infty} a_k^2 \lambda_k (1 - \lambda_k)^{2n+1}. \tag{29}$$

Hence [see (21)],

$$I_n \le \frac{1}{4} \sum_{k=0}^{\infty} a_k^2 (1 - \lambda_k)^{2n} = E_n/4 \tag{30}$$

because $\lambda_k(1 - \lambda_k) < \frac{1}{4}$. If, at the nth-iteration step, the energy I_n computed from (29), is large, then, the energy E_n of the error is also large. However, if I_n is small, E_n is not necessarily small. The inequality

$$E_{n+1} < \frac{\lambda_n}{1 - \lambda_n} I_n + \sum_{k>n} a_k^2 \tag{31}$$

obtained readily from (21) and (29), gives an upper bound for E_{n+1} but this is useful only if some information about the speed of convergence of the series (11) is available.

Suppose, finally, that $F(\omega) = 0$ for $|\omega| > \omega_0$ but the precise value of ω_0 is not given. In this case, the following must be considered in the selection of the cutoff frequency σ. If σ is large, then $1 - \lambda_k$ is small; however, this does not lead to a reduction of the error E_n because an increase of σ beyond ω_0 results in an increase of the coefficients a_k. If σ is smaller than ω_0, then as we show next, aliasing errors result. The optimum σ is a number close to ω_0 from above.

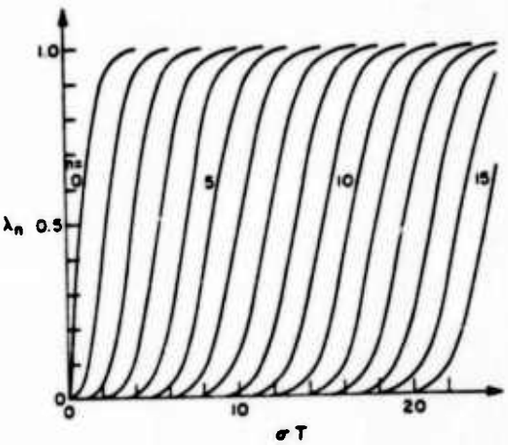

Fig. 5. First 15 eigenvalues λ_n of the integral equation

$$\int_{-T}^{T} \phi(\tau) \frac{\sin \sigma(t - \tau)}{\pi(t - \tau)} \, d\tau = \lambda \phi(t).$$

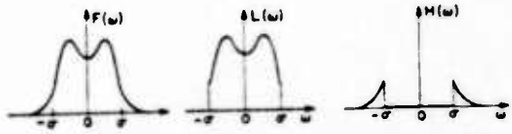

Fig. 6. Low- and high-frequency components of $F(\omega)$.

Aliasing Error

The convergence of $f_n(t)$ to the function $f(t)$ is based on the assumption that $F(\omega) = 0$ for $|\omega| > \sigma$. If $f(t)$ is not band-limited, then this is no longer true. However, as we shall show, the iteration properly terminated yields a useful estimate of $F(\omega)$ as long as the energy E_h of the high-frequency component $h(t)$ of $f(t)$ is sufficiently small.

We introduce the functions (Fig. 6)

$$L(\omega) = \begin{cases} F(\omega), & |\omega| \le \sigma \\ 0, & |\omega| > \sigma \end{cases}$$

$$H(\omega) = \begin{cases} 0, & |\omega| \le \sigma \\ F(\omega), & |\omega| > \sigma \end{cases} \tag{32}$$

and their inverse transforms $l(t)$ and $h(t)$. Clearly,

$$F(\omega) = L(\omega) + H(\omega)$$

$$f(t) = l(t) + h(t).$$

The iteration scheme is obviously linear in $f(t)$; therefore, $f_n(t)$ can be written as a sum

$$f_n(t) = l_n(t) + h_n(t) \tag{33}$$

where $l_n(t)$ and $h_n(t)$ are the contributions due to $l(t)$ and $h(t)$, respectively. As we see from (32), the function $l(t)$ is band-limited; hence, the component $l_n(t)$ of $f_n(t)$

tends to $I(t)$ with $n \to \infty$. It suffices, therefore, to examine the behavior of $h_n(t)$.

We expand the function $h(t)$ into a series in the interval $(-T,T)$

$$h(t) = \sum_{k=0}^{\infty} c_k \phi_k(t), \qquad |t| \le T \tag{34}$$

[see (69)]. Clearly,

$$\sum_{k=0}^{\infty} c_k^2 \lambda_k = \int_{-T}^{T} h^2(t)\, dt < E_h = \frac{1}{2\pi} \int_{|\omega| > \sigma} |F(\omega)|^2\, d\omega. \tag{35}$$

From (17) it follows that

$$h_n(t) = \sum_{k=0}^{\infty} c_k(1 - \mu_k^n)\phi_k(t), \qquad \mu_k = 1 - \lambda_k. \tag{36}$$

The function $h_n(t)$ is band-limited by construction and its energy equals

$$E_{nh} = \sum_{k=0}^{\infty} c_k^2(1 - \mu_k^n)^2 = \sum_{k=0}^{\infty} c_k^2 \lambda_k^2 (1 + \mu_k + \cdots + \mu_k^{n-1})^2. \tag{37}$$

The numbers λ_k and μ_k are positive and less than 1; hence,

$$1 + \mu_k + \cdots + \mu_k^{n-1} < n$$

and

$$E_{nh} < n^2 \sum_{k=0}^{\infty} c_k^2 \lambda_k = n^2 E_h. \tag{38}$$

The above bound is too pessimistic; the actual value of E_{nh} might be considerably smaller.

Noise and Roundoff Error

Suppose that for $|t| < T$, the known signal is a sum

$$g(t) + y(t) \tag{39}$$

where $y(t)$ is a random process with autocorrelation

$$E\{y(t_1)y(t_2)\} = R(t_1,t_2).$$

At the nth iteration, $f_n(t)$ is replaced by $f_n(t) + x_n(t)$ where the random component $x_n(t)$ is due to $y(t)$. We shall assume that the noise $y(t)$ is white as in (78)

$$R(t_1,t_2) = Sp_T(t_1)\delta(t_1 - t_2). \tag{40}$$

We expand the transform

$$Y(\omega) = \int_{-T}^{T} y(t)e^{-j\omega t}\, dt \tag{41}$$

of $y(t)$ into a Karhunen–Loeve series in the interval $(-\sigma,\sigma)$ [see (74), (80), and (25)]

$$X_1(\omega) = Y(\omega)p_\sigma(\omega) = Bp_\sigma(\omega) \sum_{k=0}^{\infty} d_k \sqrt{\lambda_k}\, \phi_k(b\omega). \tag{42}$$

It is not difficult to see from (75) that

$$E\{d_k d_r^*\} = \begin{cases} S/\lambda_k, & k = r \\ 0, & k \ne r \end{cases} \tag{43}$$

$$E\{|X_1(\omega)|^2\} = 2S\pi b \sum_{k=0}^{\infty} \phi_k^2(b\omega) = 2ST. \tag{44}$$

The nth-iteration function $X_n(\omega)$ is given by the right side of (26) where the coefficients a_k are replaced by d_k. Hence, its mean-square value R_n is given by

$$R_n = E\{|X_n(\omega)|^2\} = 2S\pi b \sum_{k=0}^{\infty} \left[\frac{1 - (1 - \lambda_k)^n}{\lambda_k}\right]^2 \phi_k^2(b\omega) = 2S\pi b \sum_{k=0}^{\infty} (1 + \mu_k + \cdots + \mu_k^{n-1})^2 \phi_k^2(b\omega). \tag{45}$$

This error is similar to the aliasing error E_{nh} in (37) and it is bounded by

$$R_n \le 2STn^2 \tag{46}$$

as in (38).

The preceding analysis can be used to determine the effect of the roundoff error on the estimate $F_n(\omega)$ of $F(\omega)$. In the evaluation of the Fourier transform $G(\omega)$ of $g(t)$ by a sum, roundoff errors are introduced. If these errors are independent with standard deviation σ (smallest available digit), then, their effect on $F_n(\omega)$ is approximately equivalent to the presence of a noise term $y(t)$ as in (39) with $S = \sigma^2\delta$ where δ is the sampling interval. The resulting mean-square error at the nth iteration is given by R_n as in (45). Similarly, the roundoff error introduced at the kth-iteration step causes a mean-square error in the evaluation of $F_n(\omega)$ equal to R_{n-k}.

V. Comparison with the Prolate Spheroidal Expansion Method

We shall discuss briefly the method of prolate expansion for determining $F(\omega)$ from $g(t)$ and will compare it with our approach.

We expand the tir -limited function $g(t)$ into a series as in (69). The coefficients a_k are given by

$$a_k = \frac{1}{\lambda_k} \int_{-T}^{T} g(t)\phi_k(t)\, dt. \tag{47}$$

We insert the numbers so obtained in the expansion (11). The resulting sum $f(t)$ equals the band-limited extrapolation $f(t)$ of the piece $g(t)$. The transform $F(\omega)$ of $f(t)$ is obtained from (25)

$$F(\omega) = B \sum_{k=0}^{\infty} \frac{a_k}{\sqrt{\lambda_k}} \phi_k(b\omega), \qquad |\omega| \le \sigma. \tag{48}$$

Thus to evaluate $F(\omega)$ with this method, we must store the sample values of the functions $\phi_k(t)$ and use them to evaluate the integral in (47). Our method involves only discrete Fourier series and makes use of available algorithms and the $N \log N$ economy of the FFT.

In most applications, the product σT is large. This assumption does not reduce the computations in the prolate method. In our method it leads to a rapid convergence that can be sensed by computing E_{nh}.

If noise or aliasing errors are present, no method permits the precise evaluation of $F(\omega)$. An approximate result is possible with the prolate method if the series (48) is truncated. In our approach, the iteration must be carried out to a value n such that the errors E_{nh} and R_n in (37) or (45) are sufficiently small. If n is too small, the truncation error E_n [see (28)] might be unacceptable. In a specific example, a compromise must be sought; the bounds (30), (38), and (46) give some guidance.

VI. Relationship to Frequency-Dependent Windows and Integral Equations

In the proposed iteration, the function $F_n(\omega)$ of the nth step is a linear functional of the segment $g(t)$. We denote by $y(\omega,\tau)$ the limit of $F_n(\omega)$ corresponding to $g(t) = \delta(t - \tau)$. Since

$$g(t) = \int_{-T}^{T} g(\tau)\delta(t - \tau)\, d\tau$$

it follows from the linearity of the iteration that

$$F(\omega) = \int_{-T}^{T} g(\tau)\, y(\omega,\tau)\, d\tau. \tag{49}$$

With

$$w(\omega,t) = y(\omega,t)e^{j\omega t}$$

(49) yields

$$F(\omega) = \int_{-T}^{T} w(\omega,t)\, g(t)e^{-j\omega t}\, dt. \tag{50}$$

This is of the form (3) with the difference that the window $w(\omega,t)$ is frequency dependent. Unlike the estimate $F_w(\omega)$ in (3), the inverse of $F(\omega)$ in (50) is not zero for $|t| > T$ but it equals the unknown segment of $f(t)$.

We shall next show that the function $y(\omega,\tau)$ in (49) is the Fourier transform of the resolving kernel of an integral equation. Since $f(t) = g(t)$ for $|t| < T$, the Fourier transform $F(\omega)$ of $f(t)$ can be written as a sum

$$F(\omega) = \int_{|t|<T} g(t)e^{-j\omega t}\, dt + \int_{|t|>T} f(t)e^{-j\omega t}\, dt. \tag{51}$$

But $F(\omega) = 0$ for $|\omega| > \sigma$ by assumption; hence,

$$\int_{|t|>T} f(t)e^{-j\omega t}\, dt = -\int_{-T}^{T} g(t)e^{-j\omega t}\, dt, \quad \text{for } |\omega| > \sigma. \tag{52}$$

This is a linear integral equation for the unknown segment of $f(t)$. Denoting by $k(t,\tau)$ its resolving kernel, we obtain

$$f(t) = \int_{-T}^{T} g(\tau)k(t,\tau)\, d\tau. \tag{53}$$

Taking Fourier transforms of both sides of (53) we obtain (49) where

$$y(\omega,\tau) = \int_{-\infty}^{\infty} k(t,\tau)e^{-j\omega t}\, dt. \tag{54}$$

The discrete form of (52) is a system of linear equations.

Appendix A

The Method of Maximum Entropy

In the numerical evaluation of $F(\omega)$, the integral in (1) is replaced by a sum

$$F(\omega) = \sum_{n=-\infty}^{\infty} f_n e^{-jna\omega}, \qquad f_n = af(na). \tag{55}$$

This is the exact if $F(\omega) = 0$ for $|\omega| > \pi/a$. Otherwise, it is approximate subject to aliasing errors. Since only the segment $g(t)$ of $f(t)$ is known, the above sum must be estimated in terms of its $2M + 1$ coefficients

$$f_n = g_n = ag(na), \qquad |n| \le M = [T/a]. \tag{56}$$

The method of maximum entropy is developed for the estimation of power spectra [11], [12]. In this case, $F(\omega)$ is real and positive. The function $F(\omega)$ is so selected as to maximize the integral (entropy)

$$\int_{-\pi/a}^{\pi/a} \log F(\omega)\, d\omega$$

subject to the $2M + 1$ constraints (56). It is easy to show that [13], this assumption leads to the conclusion that $F(\omega)$ must be rational with no finite zeros. Since $F(\omega) \ge 0$, it follows from the Fejer–Riesz theorem [5] that

$$F(\omega) = \frac{p}{\left|1 + \sum_{k=1}^{M} y_k e^{-jka\omega}\right|^2} \tag{57}$$

where all the zeros z_i of the polynomial

$$Y(z) = 1 + \sum_{k=1}^{M} y_k z^{-k}$$

are inside the unit circle.

Our problem is thus reduced to the determination of the $M + 1$ constants $p, y_1, \cdots, y_m$. The number of independent equations in (56) is also $M + 1$ because $f_{-n} = f_n^*$.

We maintain that

$$\sum_{k=1}^{M} g_{n-k}y_k = -g_n, \qquad n = 1, \cdots, M \tag{58}$$

and

$$p = g_0 + \sum_{k=1}^{M} g_{-k}y_k. \tag{59}$$

Thus to find the y_k's we solve the system (58). The special form g_{n-k} of the coefficient matrix (Toeplitz) simplifies the computations. Inserting the solution into (59), we obtain the constant p.

Proof: With

$$H(z) = \sum_{n=-\infty}^{\infty} f_n z^{-n} \tag{60}$$

we have [see (55)] $F(\omega) = H(e^{j\omega a})$ and (57) yields

$$H(z)\left(1 + \sum_{k=1}^{M} y_k z^{-k}\right) = \frac{p}{1 + \sum_{k=1}^{M} y_k^* z^k}. \tag{61}$$

The zeros $1/z_i^*$ of the denominator $Y^*(1/z^*)$ of (61) are outside the unit circle, hence, the inverse z-transform of the right side of (61) is zero for $n > 0$ and it equals p for $n = 0$. Equating the inverse z-transforms of both sides, we obtain

$$f_n + \sum_{k=1}^{M} f_{n-k} y_k = \begin{cases} p, & n = 0 \\ 0, & n > 0 \end{cases}. \tag{62}$$

The above yields (58) for $n = 1, \cdots, M$ [see (56)] and (59) for $n = 0$.

We note that the maximum entropy method can be considered as a method of estimating $F(\omega)$ in terms of g_n with the *a priori* assumption (Class 2)) that $F(\omega)$ is of the form (57).

Appendix B

The Prolate Spheroidal Functions

The eigenfunctions $\phi_k(t)$ of the equation

$$\int_{-T}^{T} \phi(\tau) \frac{\sin \sigma(t-\tau)}{\pi(t-\tau)}\, d\tau = \lambda \phi(t) \tag{63}$$

known as prolate spheroidal wave functions [7], are orthogonal in the intervals $(-\infty,\infty)$ and $(-T,T)$

$$\int_{-\infty}^{\infty} \phi_i(t)\phi_k(t)\, dt = \begin{cases} 1, & i = k \\ 0, & i \neq k \end{cases}$$

$$\int_{-T}^{T} \phi_i(t)\phi_k(t)\, dt = \begin{cases} \lambda_k, & i = k \\ 0, & i \neq k \end{cases} \tag{64}$$

The eigenvalues λ_k are such that

$$1 > \lambda_0 > \cdots > \lambda_k > \cdots > 0 \quad \text{and} \quad \lambda_k \to 0, \quad \text{with } k \to \infty. \tag{65}$$

The functions $\phi_k(t)$ equal their own Fourier transforms properly truncated and scaled:

$$\phi_k(t) \leftrightarrow \frac{B}{\sqrt{\lambda_k}} \phi_k(b\omega) p_\sigma(\omega), \qquad B = \sqrt{2\pi T/\sigma}, \quad b = T/\sigma$$

$$\phi_k(t) p_T(t) \leftrightarrow B\sqrt{\lambda_k}\, \phi_k(b\omega). \tag{66}$$

Thus the solutions of (63) are band-limited hence,

$$\int_{-\infty}^{\infty} \phi_k(\tau) \frac{\sin \sigma(t-\tau)}{\pi(t-\tau)}\, d\tau = \phi(t). \tag{67}$$

A band-limited function $f(t)$ can be expanded into a series in the interval $(-\infty,\infty)$

$$f(t) = \sum_{k=0}^{\infty} a_k \phi_k(t)$$

$$a_k = \int_{-\infty}^{\infty} f(t)\phi_k(t)\, dt. \tag{68}$$

An arbitrary function $g(t)$ can be expanded into a series in the interval $(-T,T)$

$$g(t) = \sum_{k=0}^{\infty} a_k \phi_k(t)$$

$$a_k = \frac{1}{\lambda_k} \int_{-T}^{T} g(t)\phi_k(t)\, dt. \tag{69}$$

From the above and (64) we conclude that

$$\int_{-\infty}^{\infty} f^2(t)\, dt = \sum_{k=0}^{\infty} a_k^2$$

$$\int_{-T}^{T} g^2(t)\, dt = \sum_{k=0}^{\infty} a_k^2 \lambda_k. \tag{70}$$

We, finally, note that

$$\sum_{k=0}^{\infty} \phi_k^2(t)\, dt = \sigma/\pi. \tag{71}$$

This follows by expanding the band-limited function $\sin \sigma(t-x)/\pi(t-x)$ into a series as in (68) and using (63).

Appendix C

The Karhunen–Loève Expansion

Consider a stochastic process $y(t)$ with autocorrelation

$$R(t_1,t_2) = E\{y(t_1)y^*(t_2)\}.$$

With

$$\Gamma(u,v) = E\{Y(u)Y^*(v)\}$$

the autocorrelation of the Fourier transform $Y(\omega)$ of $y(t)$, it is easy to show that [14]

$$\Gamma(u,v) = \int_{-\infty}^{\infty}\int_{-\infty}^{\infty} R(t_1,t_2) \exp\left(-j(ut_1 - vt_2)\right) dt_1\, dt_2. \tag{72}$$

With $\Gamma(u,v)$ as above, we form the equation

$$\int_{-\sigma}^{\sigma} \Gamma(u,v)\psi(v)\, dv = \gamma\psi(u) \tag{73}$$

and denote by $\psi_k(u)$ and γ_k its eigenfunctions and eigenvalues. It can be shown that in the expansion

$$Y(\omega) = \sum_{k=0}^{\infty} z_k \psi_k(\omega), \qquad |\omega| \leq \sigma \tag{74}$$

the random variables z_k are orthogonal [14] and

$$E\{z_i z_k^*\} = \begin{cases} \gamma_k, & i = k \\ 0, & i \neq k \end{cases}. \tag{75}$$

Nonstationary white noise: We say that the process $y(t)$ is white noise if

$$R(t_1,t_2) = q(t_1)\delta(t_1 - t_2) \tag{76}$$

where $q(t) \geq 0$ is its "average intensity." With $Q(\omega)$ the Fourier transform of $q(t)$, it follows from (72) that

$$\Gamma(u,v) = Q(u - v). \tag{77}$$

If $y(t) = n(t)p_T(t)$ and $n(t)$ is stationary white noise with autocorrelation $S\delta(t_1 - t_2)$, then

$$R(t_1,t_2) = Sp_T(t_1)\delta(t_1 - t_2). \tag{78}$$

In this case,

$$q(t) = Sp_T(t) \qquad Q(\omega) = 2S \sin T\omega/\omega. \tag{79}$$

From the above and (77) it follows that the integral equation (73) takes the form

$$2S \int_{-\infty}^{\infty} \frac{\sin T(u - v)}{u - v} \psi(v)\, dv = \gamma\psi(u). \tag{80}$$

As we see from (63), its eigenfunctions $\psi_k(u)$ equal the prolate spheroidal functions $\phi_k(t)$ properly scaled.

References

[1] R. B. Blackman and J. W. Tukey, *The Measurement of Power Spectra*. New York: Dover, 1958.
[2] G. M. Jenkins and D. G. Watts, *Spectral Analysis and Its Applications*. San Francisco, Calif.: Holden-Day, 1968.
[3] A. Papoulis, "Minimum bias windows for high-resolution spectral estimates," *IEEE Trans. Inform. Theory*, vol. IT-19, pp. 9–12, Jan. 1973.
[4] T. P. Burg, "Maximum entropy spectral analysis," presented at the 37th Int. SEG Meeting, Oct. 1967.
[5] N. I. Akhiezer, *Theory of Approximations*. New York: Ungar, 1956.
[6] R. W. Gerchberg, "Super-resolution through error energy reduction," *Optica Acta*, vol. 21, no. 9, pp. 709–720, 1974.
[7] D. Slepian, H. O. Pollak, and H. J. Landau, "Prolate spheroidal wave functions," *Bell Syst. Tech. J.*, vol. 40, pp. 43–84, Jan. 1961.
[8] A. Papoulis, *The Fourier Integral and Its Applications*. New York: McGraw-Hill, 1962.
[9] A. Papoulis, "Limits on bandlimited signals," *Proc. IEEE*, vol. 55, pp. 1677–1686, Oct. 1967.
[10] D. Slepian and E. Sonnenblick, "Eigenvalues associated with prolate spheroidal wave functions of zero order," *Bell Syst. Tech. J.*, vol. 44, pp. 1745–1759, Oct. 1965.
[11] R. T. Lacoss, "Data adaptive spectral analysis methods," *Geophys.*, vol. 86, pp. 661–675, 1971.
[12] T. J. Ulrych, "Maximum entropy power spectrum of truncated sinusoids," *J. Geophys. Res.*, vol. 77, pp. 1396–1400, 1972.
[13] J. A. Edward and M. M. Fitelson, "Notes on Maximum-entropy processing," *IEEE Trans. Inform. Theory*, vol. IT-19, pp. 232–234, Mar. 1973.
[14] A. Papoulis, *Probability, Random Variables, and Stochastic Processes*. New York: McGraw-Hill, 1965.

Athanasios Papoulis (S'47–SM'55–F'67) studied at the Polytechnic Institute of Athens, Athens, Greece, and at the University of Pennsylvania, Philadelphia.

He taught at the University of Pennsylvania, at Union College, and since 1952, he has been teaching at the Polytechnic Institute of Brooklyn (now PINY), Farmingdale, N.Y. He was a visiting Professor at the Technische Hochschule Darmstadt, Darmstadt, Germany, at the University of California, Los Angeles, and at Stanford University, Stanford, Calif.

UNSTABLE RESONATORS

L. Felsen

As noted in the proposal, we have developed a new method of analysis of empty unstable resonator cavities whereby the finite mirror configuration is regarded as a waveguide in the direction transverse to the resonator axis. Invoking coupling, at the mirror edges, between two appropriate waveguide modes, we have been able to explain in a quantitative manner[1] the intricate behavior of the eigenmode loss curves, which have been furnished in the literature by numerical solution of the resonator integral equation[2,3].

The effort during the current period has been directed along two lines: a) to further solidify the basic approach so as to make it applicable also to mirror configurations other than the hyperbolic shape considered so far; and b) to extend the analysis to resonators filled with inhomogeneous and active material.

On item a), we have completed a detailed study of the modal resonance equation to determine the eigenmode loss characteristics of symmetrical resonators with cylindrical and spherical mirrors of hyperbolic shape. We have then shown that the waveguide model can be applied as well to other mirror configurations (asymmetrical, telescopic, etc.) and that the properties of these structures can be related to those of the symmetrical hyperbolic type. The equivalence relations so derived from the waveguide model agree with those presented in the literature from considerations involving the resonator integral equation. This serves as further substantiation of the validity of the waveguide model. The results of this study have been prepared in the form of a manuscript which is to be published in the Applied Optics Issue of the Proceedings of the 1975 CLEA[4].

An essential part of the waveguide approach is the separation of the overall resonator behavior into "canonical" constituents which highlight the separate roles played by edge diffraction and by propagation between the edges and the resonator interior. The geometric optical nature of the edge diffraction process, and its influence on the eigenmode fields and losses, has been recognized and conjectured but has not previously been incorporated into a quantitative theory. We have applied and generalized a previously developed ray-optical theory[5] for scattering by edge discontinuities

in waveguides to show the adequacy of the geometric-optic edge diffraction mechanism at large Fresnel numbers. We have also shown the transition from this regime to that of small Fresnel numbers where edge diffraction is more appropriately described by a local open-ended parallel plane waveguide model. These new results accommodate the entire range of parameters from large to small Fresnel numbers within the same quantitative format based on the waveguide approach.

On item b), work has been initiated on two-dimensional parallel plane resonators filled with a medium that is inhomogeneous in the direction transverse to the resonator axis. The parallel plane configuration was chosen initially to permit separability of the wave equation in the inhomogeneously filled region. A principal goal of this study is to assess the separate influence of the mirror edges and the medium profile (both refractive index and gain) on the resonator behavior. The problem is being formulated for arbitrary (though slowly varying, over a wavelength interval) profile shapes by recourse to WKB and uniform asymptotic methods available from the theory of differential equations.

References

1. L.W. Chen and L.B. Felsen, IEEE J. Quant. Electron. QE-9, 1102, 1973.
2. R.L. Sanderson and W. Streifer, Appl. Opt. 8, 2129 (1969).
3. A.E. Siegman and H.Y. Miller, Appl. Opt. 9, 2729 (1970).
4. C. Santana and L.B. Felsen, "Unstable Resonators -- Two-Dimensional and Three-Dimensional Losses by a Waveguide Analysis", to be published in CLEA Special Issue of Applied Optics.
5. D.V. Batorsky and L.B. Felsen, Radio Sci. 6, 911 (1971).

METAL SCREENING PROGRAM

Vapors of atoms with suitable low-lying energy level structures can provide active media for efficient, pulsed gas-discharge or possibly chemical lasers.[1] The goal of the metal screening program is to investigate these metallic vapors as the active media for more efficient lasers in the visible and ultraviolet spectral regions. A three phase program is being pursued consisting of:

1. System Evaluation
2. Computer Modeling
3. Experimental Investigation

1. In the initial evaluation the criteria developed earlier[1] concerning the ordering, spacing and parity of energy levels, atomic transition probabilities and branching ratios were applied to all the elements. The most promising possibilities for the ultraviolet and blue-green spectral regions are listed below:

Ultraviolet Candidates

2414 Å Selenium
2770 Å Tellurium

Blue-Green Candidates

4685 Å Germanium
4722 Å Bismuth
4942 Å Chromium

These candidate laser transitions were selected for two reasons: first, their wavelengths are in spectral regions of strong interest; and second, the 2414 Å selenium, 2770 Å tellurium and 4942 Å chromium lines have transition probabilities which are smaller than that of the similar 5105 Å copper vapor laser transition. A low value of the proposed laser line's atomic transition probability is important because of the superradiance limitation on this class of pulsed self-terminating or cyclic lasers. For the cyclic laser in copper vapor we have measured a small signal gain coefficient of 4 dB/cm on the 5105 Å transition. With such a large gain, superradiance (or better superfluorescence) is the limiting process in scaling the copper vapor laser. If cyclic lasers can be developed on transitions with smaller atomic transition probabilities, higher densities or larger volumes could be utilized before reaching this limit. The proposed cyclic laser transition at 4942 Å in chromium, for example, has a transition probability of 4×10^5 which is five times lower than that of copper.

The atomic energy levels of Moore [2] and the atomic transition probabilities of Corliss and Bozman [3] have been used in this initial evaluation. Although the work of Corliss and Bozman is the broadest treatment of atomic transition probabilities presently available, errors as large as a factor of 20 have been found when their values have been compared with more-accurate measured values. Because the Corliss-Bozman values remain the only consistent set of transition probabilities spanning the stronger spectral lines of most of the solid elements, there has been considerable interest in attempting to improve these values.

Accurate values of atomic transition probabilities are most important in the evaluation of new, efficient laser systems. Therefore as part of the metal screening program we have explored the possibility of improving the Corliss-Bozman values of atomic transition probabilities. A procedure was developed to obtain improved transition probabilities from the spectral line intensities of Meggers, Corliss and Scribner by applying a correction to the temperature of the Meggers-Corliss-Scribner arc and by incorporating each element's partition function in the procedure. This procedure is described in Appendix I. In Appendix I the temperature of the Meggers-Corliss-Scribner arc is shown to be closer to 6200°K than the 5100°K they assumed. Recently the NBS group published a revised set of spectral line intensities. [4] These revised intensities are now being analysed to refine the procedure and develop a table of improved atomic transition probabilities for transition of interest as potential efficient laser candidates.

2. A computer model of the dynamics of these cyclic lasers has been developed and is now being refined. The goal is to increase our understanding of the importance of various physical processes involved as well as to provide insight on scaling these lasers. The computer model is described in Appendix II. Thus far the model has been applied to two metal vapor laser systems: 1) the copper vapor system - to compare the model's predictions with the actual performance of our copper vapor lasers, and 2) the bismuth vapor system- to analyse the effect of and assess the importance of processes which compete with the basic laser dynamics.

During the development phase of the computer model, the model was tested on two copper vapor laser geometries. Qualitative agreement was obtained between the model predictions and the experimental measurements but

a detailed comparison has not yet been carried out. Attention was shifted to the bismuth vapor system where cyclic laser action has not been observed at 4722 Å in spite of demonstration attempts at various laboratories including the Polytechnic.[5] Because bismuth has three valence electrons, there are more excitation paths available in a bismuth discharge than in the single valence electron system in copper. Cascade filling of the lower laser level is also more likely to be a detrimental process in bismuth vapor.

To examine the question of whether these competing processes could account for the absence of laser action in bismuth vapor, the computer model was modified to include electron excitation to and spontaneous radiation from fifteen levels of the bismuth atom. Atomic energy levels of Moore[2] and transition probabilities of Corliss and Bozman were used. Electron excitation and ionization cross sections were estimated using the semiclassical formulas of Gryzinski.[6]

For our experimental conditions the model predicted that a population inversion would be achieved and laser action at 4722Å would result in the bismuth vapor discharge. The competing processes therefore did not appear to be sufficiently detrimental to prevent laser action. In May of 1975 the electron impact measurement by Williams, Trajmar and Bozinis (WTB)[7] of the electron excitation cross section at 40 eV of the upper $^4P_{1/2}$ and lower $^2D_{3/2}$ bismuth levels became available. At 40 eV our Gryzinski estimate of the cross section of the upper laser level ($^4P_{1/2}$) was approximately one-half that of the WTB value and our Gryzinski estimate of the cross section for electron excitation to the lower laser level ($^2D_{3/2}$) was approximately $^1/_{30}$ that of the WTB value. We then used these WTB values to normalize our relative Gryzinski excitation curves; that is, we increased our upper laser level excitation rates by a factor of 2 and our lower level excitation rates by a factor of 30 throughout the energy range. Still the computer model predicted laser action at 4722 Å with a 30 kW peak output power under conditions which correspond to those of our apparatus. Thus far, then, competing processes do not appear to account for the absence of laser action in bismuth vapor.

The computer model is now being refined. Reaction processes, including dimer formation and multiple ionization, are being incorporated into the model. Attention is also being directed to the initial nanosecond during which the electron temperature in the model rises to unphysically high values (10^6 eV). The interplay of experimental results with computer model predictions greatly facilitates the progress in understanding the importance of the physical processes involved.

3. Experimental work is underway on both the selenium and the germanium vapor systems. Selenium is strongly electronegative, lying under oxygen in the periodic table. When the vapor pressure of selenium reached ~10mtorr in our conventional, longitudinal-discharge, metal vapor-rare gas mixture systems, the discharge extinguished and could not be reestablished with voltages as high as 20 kV. Shorter longitudinal-discharges were tried without success. Obviously systems with higher values of E/p are required. We are now constructing a transverse-discharge system to overcome this problem. Shaped electrodes have been constructed and preionization will be utilized to establish a uniform, large-area discharge. The initial testing of this new transverse-discharge system will be carried out at room temperature with a nitrogen fill. The pulsed nitrogen laser at 3371 Å is a similar self-terminating transition which can be used to test and calibrate the new apparatus.

Our initial examination of germanium vapor for laser action at 4685 Å has been quite promising. Unlike bismuth, germanium is transparent at the proposed laser wavelength. Blocking the back mirror produces a decrease in the detection signal at 4685 Å. The hot zone available in the metal vapor system used was ~ 12 cm long. The germanium vapor system will next be examined in a metal vapor system where a longer hot zone is available (~ 80 cm).

Chromium is also a promising candidate to test in the longer metal vapor facility. As already mentioned above, the Corliss-Bozman value for the transition probability of the 4942 Å proposed laser line is 5 times smaller than that of the green 5105Å transition in copper vapor. Therefore the superradiance limitation will be less severe in chromium than in copper.

In conclusion then, a three phase effort is being carried out in the screening of metal vapors for efficient visible and ultraviolet laser systems. System evaluation has identified several promising candidates. A procedure has been developed to improve the values of atomic transition probabilities determined from spectral lineintensities. A computer model of these pulsed metal vapor systems has been developed. The model is being refined to determine the importance of various physical processes, complete the evaluation of the candidate metallic vapor systems and examine the scaling of these systems. Experimentally selenium and germanium vapor systems are undergoing further examination - selenium in a transverse discharge and germanium in a longer longitudinal discharge. Chromium will also be examined in the longer longitudinal discharge. It is recommended that this work be supported for another year to carry out these evaluations.

References

1. W. T. Walter, N. Solimene, M. Piltch and G. Gould, "Efficient Pulsed Gas Discharge Lasers," IEEE J. Quantum Electron. QE-2, 474-9 (1966).

2. C. E. Moore, "Atomic Energy Levels," National Bureau of Standards Circular 467 (Washington, D. C.: U. S. Government Printing Office, Vol. 1, 1949, Vol. 2, 1952, Vol. 3, 1958).

3. C. H. Corliss and W. R. Bozman, "Experimental Transition Probabilities for Spectral Lines of Seventy Elements," National Bureau of Standards Monograph 53 (Washington, D. C.: U. S. Government Printing Office, 1962).

4. W. F. Meggers, C. H. Corliss and B. F. Scribner, "Tables of Spectral-Line Intensities," 2nd Ed., National Bureau of Standards Monograph 145 (Washington, D. C.: U. S. Government Printing Office, 1975).

5. K. Park, N. Solimene and W. T. Walter, "Investigation of Cyclic Laser Action in Bismuth Vapor," Progress Report No. 38 to JSTAC, Polytechnic Institute of New York, Report No. R-452.38-73 (1973).

6. M. Gryzinski, "Classical Theory of Atomic Collisions. I. Theory of Inelastic Collisions," Phys. Rev. 138A, 336-58(1965); also, A. E. S. Green, "Electron Impact Cross Sections for Aeronomy," AIAA J., 4, 769-75 (1966).

7. W. Williams, S. Trajmar and D. G. Boyimis, "Elastic and Inelastic Scattering of 40 eV Electrons from Atomic and Molecular Bismuth", J. Phys. B: Atom. Molec. Phys. 8, L96-9 (1975).

APPENDIX I

IMPROVED VALUES OF ATOMIC TRANSITION PROBABILITIES

W. T. Walter and N. Solimene

The rate at which an appropriately excited atom or molecule spontaneously radiates in a particular spectral line is characterized by a transition probability, $A_{u\ell}(sec^{-1})$, which is sometimes referred to as the Einstein A coefficient. The wavelength of the spectral line is related to the energies of the upper (u) and lower (ℓ) levels, $\lambda = hc/(E_u - E_\ell)$. Accurate values of these transition probabilities are required whenever the kinetics of processes involving excited states of atoms or molecules are examined; for example, in the search for more efficient visible and ultraviolet lasers, in the study of chemical reactions, for astrophysical determinations of solar abundances, interstellar cloud composition, etc.

Transition probabilities can be both calculated and measured. They can be calculated from first principles only for the lightest elements, but the calculations may be extended to heavier elements by including experimental parameters. Experimental measurements of transition probabilities can be divided into two classes; (1) methods which require knowledge of the density of the radiating species, such as the hook method of Rozhdestvenskii and emission and absorption techniques, and (2) methods which are independent of the vapor density such as level crossing, optical double resonance and phase shift techniques. Only these latter measurement methods can be relied upon to give values with an absolute accuracy approaching 10%. Beam foil spectroscopy can be included with these more accurate methods if one can be certain that there is no unrecognized cascading from higher levels.

Although recent work has produced more accurate values of some spectral lines in selected elements, the work of Corliss and Bozman[1] remains the broadest treatment of transition probabilities presently available. Corliss and Bozman used the spectral line intensities measured by Meggers, Corliss and Scribner[2] to calculate transition probabilities of some 25,000 classified lines in 70 elements. Meggers, Corliss and Scribner had measured the peak intensities, I, of 39,000 spectral lines radiated from free-burning 10A dc arcs in air between electrodes of copper to which 1 atom in 1000 of the element of interest had been added. Unfortunately when the Corliss and Bozman values are compared with the more accurate values determined by density-independent methods, errors as large as a factor of 20 have been found. There is therefore a widespread reluctance to use the Corliss and Bozman values, although in many cases they are the only ones available.

Because the Corliss and Bozman values remain the only consistent set of transition probabilities spanning the stronger spectral lines of most of the solid elements, there has been considerable interest in attempting to improve these values. Three

types of corrections have been suggested: an energy dependent correction, an intensity dependent correction and a correction in the copper arc temperature. Huber and Tobey[3] and subsequently others have shown that the energy dependent normalization function which Corliss and Bozman applied should in fact be a constant. Although originally Corliss and Bozman took the copper arc temperature to be 5100°K, Corliss[4] subsequently suggested that the temperature may actually be as high as 7000°K. Others have suggested temperature corrections. Most recently Degenkolb and Griffiths[5] suggested 6000°K on the basis of comparison with more accurate transition probabilities for the three elements Mg, Ca and Al.

In the Meggers-Corliss-Scribner arc only one atom in 1000 belongs to the element of interest; the rest are copper. When 0.1 atomic percent of the copper atoms are replaced by an element whose ionization potential[6] (IP) is close to or above that of copper (IP = 7.724 eV), the physical properties of the discharge, such as the electron distribution and temperature, should not be appreciably changed. On the other hand if the ionization potential of the added element is substantially lower than that of copper, then a noticeably lowering of the electron and arc temperatures could be observed.

For an optically thin gas, one in which effects due to self-absorption can be neglected, the intensity of the light spontaneously emitted in a particular spectral line λ due to N_u atoms in the upper energy level is

$$I = N_u A_{ul} hc/\lambda \ . \tag{1}$$

If the gas is in local thermodynamic equilibrium so that the population of the emitting atomic species can be characterized by a Boltzmann distribution, then

$$\frac{N_u}{g_u} = \frac{N_o}{g_o} e^{-E_u/kT} \tag{2}$$

where the g's represent the statistical weights of the ground (o) and upper (u) energy levels.

Now in terms of the partition function

$$U = \sum_{u=o}^{\text{all levels}} g_u e^{-E_u/kT} \tag{3}$$

and the total number of the emitting atomic species

$$N = \sum_{u=o}^{\text{all levels}} N_u = \frac{N_o}{g_o} N \ , \tag{4}$$

we can express

$$\ln \frac{I\lambda^3}{gf} = C - \frac{1}{kT} E_u \tag{5}$$

where

$$C = \frac{8\pi^2 e^2 h}{m} \frac{N}{U} \tag{6}$$

is a constant for each light-emitting species. Here the Ladenburg oscillator strength, f, has been used instead of the transition probability, $A_{u\ell}$. The relationship is

$$gf = g_\ell f_{\ell u} = g_u f_{u\ell} = \frac{mc\lambda^2}{8\pi^2 e^2} g_u A_{u\ell} = 1.499\lambda^2 g_u A_{u\ell} \tag{7}$$

If transition probabilities or f values are available for an element from one of the density-independent methods, the presence of a straight line plot of log $(I\lambda^3/gf)$ versus E_u indicates that the arc can be characterized by a Boltzmann distribution. The arc temperature can then be determined from the slope of the line. When we carried out a linear least squares analysis on such plots for elements with ionization potentials within 1 eV of that of copper, we found Boltzmann temperatures of approximately 6200°K as indicated in Table I.

In fact we find that if we take account of the different values[10] for the atomic partition functions by plotting

$$\ln \frac{I\lambda^3}{gf} U = C_1 - \frac{1}{kT} E_u \tag{7}$$

where $C_1 = CU = \frac{8\pi^2 e^2 h}{m} N$, then the points for all 129 spectral lines listed in Table I, together with those for 2 Ag spectral lines[11] (IP = 7.574eV) and 3 Pb spectral lines[12] (IP = 7.415eV) can be very satisfactorily fitted by a single Boltzmann temperature of 6230°K as shown in Figure 1. The fact that the intercept C_1 is the same for different elements indicates that the numbers of emitting atoms are the same. This corroborates Corliss and Bozman's claim that the copper electrodes diluted 1 atom in 1000 with the element of interest dispense atoms of each element into the arc at the same rate. Furthermore it indicates that demixing effects which would tend to reduce the concentration of lighter elements and those with ionization potential substantially below that of copper are not important for the elements we have examined.

Contrary to the claim of Degenkolb and Griffiths,[5] Ca and Al do not yield similar temperatures. The arc temperature does appear to decrease as the ionization potential of the added element in the Meggers-Corliss-Scribner copper arc is lowered

TABLE I. Meggers-Corliss-Scribner Arc temperatures determined from least squares analyses of the slopes of plots of log ($I\lambda^3/gf$) versus E_u.

Element	Ionization Potential[6]	Number of Spectral Lines	Ref. for f or A_{ul} Values	Arc Temperature
Fe	7.87 eV	85	7	6121°K
Cu	7.724eV	6	4 and 8	6395°K
Mg	7.644eV	19	9	6235°K
Ti	6.82 eV	19	7	6285°K

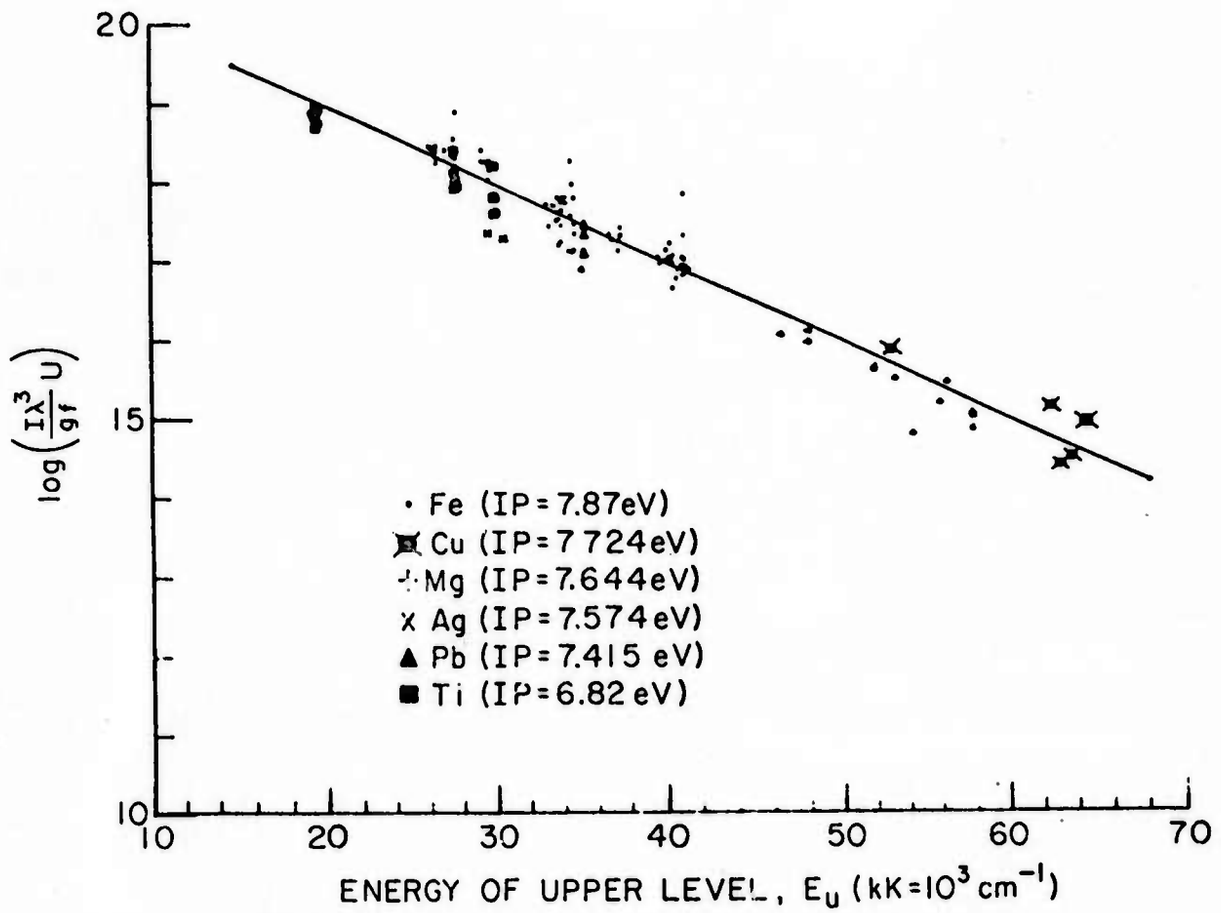

Fig. 1. Semilog plot of intensities of 134 spectral lines from 6 elements with ionization potentials within 1 eV of that of copper. The straight line least squares fit indicates a Boltzmann distribution at 6230°K for the Meggers-Corliss-Scribner arc.

more than approximately 1 eV below that of copper. For example the temperature we determined for 65 spectral lines of Ca (IP = 6.111eV) was 5037°K and for 12 spectral lines of Al (IP = 5.984eV) was 5441°K.

Therefore we suggest that for the 52 elements in the Corliss and Bozman tables with ionization potentials > 6.8eV, the temperature of the Meggers-Corliss-Scribner arc should be taken as 6230°K. In addition use of the partition function for each element will superimpose the spectral lines of all of these elements on a single Boltzmann-distribution linear semilog plot. Improved transition probabilities can then be obtained without having a single absolute transition probability measured within that element. Work is continuing at the Polytechnic to determine the range of validity of this procedure as well as to determine the increase in accuracy.

Joint Services Technical Advisory Committee
F44620-74-C-0056

W.T. Walter and N. Solimene

ARPA under Office of Naval Research Contract
N00014-67-A-0438-0017

Office of Naval Research
N00014-67-A-0438-0015

REFERENCES

1. C.H. Corliss and W.R. Bozman, "Experimental Transition Probabilities for Spectral Lines of Seventy Elements," National Bureau of Standards Monograph 53 (Washington, D.C.: U.S. Government Printing Office, 1962).

2. W.F. Meggers, C.H. Corliss and B.F. Scribner, "Tables of Spectral-Line Intensities," National Bureau of Standards Monograph 32 (Washington, D.C.: U.S. Government Printing Office, 1961). Intensities, I, taken from Ref. 2 have been multiplied by 1000 to compensate for the 0.1 atomic percentage dilution in the arc.

3. M. Huber and F.L. Tobey, "gf-Values of Ultraviolet Fe I, Cr I and Cr II Lines from Shock-Tube Measurements," Astrophys. J. 152, 609 (1968).

4. C.H. Corliss, "A Review of Oscillator Strengths for Lines of Cu I," J. Res. Nat. Bur. Stand. (U.S.), 74A, 781 (1970).

5. E.O. Degenkolb and J.E. Griffiths, "Temperature of the Meggers-Corliss-Scribner Copper Arc," J. Opt. Soc. Am. 65, 315 (1975).

6. Ionization potentials have been taken from Table 34, page xxxiv of C.E. Moore, "Atomic Energy Levels," National Bureau of Standards Circular 467 Vol. 3 (Washington, D.C.: U.S. Government Printing Office, 1958).

7. D.C. Morton and W.H. Smith, "A Summary of Transition Probabilities for Atomic Absorption Lines Formed in Low-Density Clouds," Astrophys. J. Suppl. 26, 333 (1973).

8. C.H. Corliss, "Spectral-Line Intensities and gf-Values in the First Spectrum of Copper," J. Res. Nat. Bur. Stand. (U.S.), 66A, 497 (1962). The intensities, I, of 6 spectral lines of Cu taken from Ref. 8 (4248, 4480, 4509, 4539, 4586 and 4704Å) were used directly and not multiplied by 1000 to account for dilution. Accurate transition probabilities have been determined by Kock and Richter[4] for these 6 lines which were too weak to be observed in the arc between diluted electrodes[2] but were observed in an arc between pure copper electrodes.[8] For this reason the transition probabilities of these 6 lines should be weak enough that their intensities, I, were not affected by self-absorption in a pure copper arc.

9. W. L. Wiese, M. W. Smith and B. M. Miles, "Atomic Transition Probabilities II - Sodium through Calcium," National Bureau of Standards Monograph NSRDS-NBS 22 (Washington, D. C.: U. S. Government Printing Office, 1969).

10. H. W. Drawin and P. Felenbok, "Data for Plasmas in Local Thermodynamic Equilibrium," (Paris: Gauthier-Villars, 1965).

11. P. T. Cunningham and J. K. Link, "Measurement of Lifetimes of Excited States of Na, Tl, In, Ga, Cu, Ag, Pb and Bi by the Phase-Shift Method," J. Opt. Soc. Am. 57, 1000 (1967).

12. E. B. Saloman and W. Happer, "Lifetime, Coherence Narrowing and Hyperfine Structure of the $(6s^2 6p7s)^3P_1^o$ State in Lead," Phys. Rev. 144, 7 (1966).

APPENDIX II

COMPUTER MODELING OF THE DYNAMICS OF METAL VAPOR LASERS

N. Solimene and W. T. Walter

The experimental investigation of metal vapor lasers, in particular the copper vapor laser,[1] and the search for new metal vapor lasers[2] are significant parts of the laser work at the institute. For this reason it was felt that numerical modeling of the dynamics of such lasers would be a useful adjunct to the experimental effort. Consequently a start in the development of a computer model has been made.

A. The Model

The model includes rate equations for the populations of various energy levels which are directly or indirectly involved in the development of actual or potential laser action. Also included are rate equations for the populations of additional atomic species which may be present to act as buffer gases or to facilitate electrical breakdown and discharge. The primary excitation is provided by electron collisions. De-excitation may be by electron collisions, as well as by other mechanisms such as radiative relaxation and diffusion to walls and subsequent de-excitation. The rate constants for transitions between the various energy levels and for ionization depend on the cross sections for these processes and on the electron number density and energy distribution. To simplify the model, the electron energy distribution is assumed to have a known functional form throughout the discharge pulse, but the average electron energy is permitted to change in a manner determined by an energy balance equation. Convenient distributions are the Maxwell-Boltzmann and the Druyvesteyn distribution.

This type of model has been used by Gerry[3] to investigate the pulsed molecular nitrogen laser, and by Leonard[4] to investigate the copper vapor laser.

Since in most cases the cross sections for ionization or for excitation are not known, they have been estimated using the semiclassical formulas of Gryzinski.[5] The specific rate constants are then calculated as a function of electron temperature in the Boltzmann case, or as a function of the average electron energy in the Druyvesteyn case.

The circuit equations for capacitor voltage and discharge current density are those used by Gerry and Leonard. The ohmic resistance term depends on the momentum transfer cross sections for the various species and the electron energy distribution. It is believed that the correct treatment of this term will be of some importance in correlating experimental results involving different buffer species. This will require, however, good estimates of the momentum transfer cross sections. For the present, ad hoc estimates are being used. It is hoped that classical phase shift calculations will provide better estimates which will be incorporated later on.

The ohmic resistance also enters in an ohmic heating term in the energy balance equation for the average electron energy. Other terms are energy transfer terms which describe excitation, de-excitation, and ionization. The electron number density is determined by the ionization rates for the atomic species present and by electron loss terms such as recombination. The latter are being ignored for the present since they are expected to be important only in the after-glow when the laser action is completed.

Phenomenological equations for the laser photon densities are included for each of the potential laser transitions. Output power densities may be computed using effective optical cavity time constants.

B. The Equations

1. Circuit Equations

$$\frac{dV}{dt} = -\frac{A}{C}\, j$$

$$\frac{dj}{dt} = \frac{1}{LA}\left(V - \rho \ell j\right),$$

where

V = voltage across capacitor

j = current density

C = capacitance

L = circuit inductance

ℓ = length of discharge

A = cross-sectional area of discharge

ρ = discharge resistivity.

Note that ρ depends on electron energy distribution.

2. Electron Equations

$$\frac{dN_e}{dt} = N_e \sum_k \sum_i N_i^{(k)} R_i^{(k)} ,$$

$$\frac{d}{dt}(N_e \epsilon_o) = \rho j^2 - N_e \sum_k \sum_i N_i^{(k)} R_i^{(k)} \left(E^{(k)} - E_i^{(k)}\right)$$

$$- N_e \sum_k \sum_{i,j}' N_i^{(k)} R_{ij}^{(k)} \left(E_i^{(k)} - E_j^{(k)}\right),$$

where

N_e = electron number density

ϵ_o = average electron energy

$N_i^{(k)}$ = atom number density of k^{th} component in i^{th} energy level

$E^{(k)}$ = ionization energy for k^{th} species

$E_i^{(k)}$ = energy of i^{th} level for k^{th} component

$R_i^{(k)}$ = specific electron ionization rate for k^{th} component in i^{th} energy level

$R_{ij}^{(k)}$ = specific electron excitation (de-excitation) rate from i^{th} to j^{th} level of k^{th} species.

Note that $R_i^{(k)}$ and $R_{ij}^{(k)}$ depend on electron energy distribution in a manner which is detailed below.

3. Population Equations

$$\frac{dN_i^{(k)}}{dt} = - N_e N_i^{(k)} R_i^{(k)} + N_e \sum_j \left(N_j^{(k)} R_{ji}^{(k)} - N_i^{(k)} R_{ij}^{(k)} \right)$$

$$+ \sum_j \left\{ \left(N_j^{(k)} - N_{j,eq}^{(k)} \right) \left(\frac{1}{\tau_{ji}^k} + A_{ji} \right) - \left(N_i^{(k)} - N_{i,eq}^{(k)} \right) \left(\frac{1}{\tau_{ij}^k} + A_{ij}^{(k)} \right) \right\}$$

$$+ \delta_{k,1} \sum_n \delta(n,i) B_n \left(N_{n(2)}^{(1)} - \frac{g_{n(2)}}{g_{n(1)}} N_{n(1)}^{(1)} \right) P_n ,$$

$$k = 1, 2, \ldots, c \quad , \quad i = 1, 2, \ldots, s(k) \quad ;$$

where

c = number of components in gas mixture

$s(k)$ = number of energy levels for k^{th} component

$N_{i,eq}^{(k)}$ = equilibrium number density at gas temperature

$\tau_{ij}^{(k)}$ = relaxation time for i^{th} to j^{th} level of k^{th} component due to gas or wall collisions

$A_{ij}^{(k)}$ = spontaneous emission coefficient

$n(2)$ = index for upper level of n^{th} laser transition

$N_{n(2)}^{(1)}$ = number density in upper level of n^{th} laser transition

$n(1)$ = index for lower level of n^{th} laser transition

g_j = degeneracy of j^{th} energy level in 1^{st} component

$$\delta(n,i) = \begin{cases} +1 & \text{if} \quad i = n(1) \\ -1 & \text{if} \quad i = n(2) \\ 0 & \text{otherwise} \end{cases}$$

B_n = stimulated emission coefficient for n^{th} laser transition

P_n = photon density for n^{th} laser transition.

4. Laser Photon Density Equations

$$\frac{dP_n}{dt} = - \frac{1}{\tau_n} P_n + B_n \left(N_{n(2)}^{(1)} - \frac{g_{n(2)}}{g_{n(1)}} N_{n(1)}^{(1)} \right) P_n + \frac{B_n N_{n(2)}^{(1)}}{V_n}$$

$$n = 1, 2, \ldots, n_\ell$$

where

n_ℓ = number of laser transitions

τ_n = relaxation time for n^{th} laser transition

V_n = effective mode volume .

5. Specific Rate Constants

$$R_i^{(k)} = \int_o^\infty \sigma_i^{(k)}(\epsilon) \sqrt{\frac{2\epsilon}{m}}\, f(\epsilon, \epsilon_o)\, d\epsilon$$

$$R_{ij}^{(k)} = \int_o^\infty \sigma_{ij}^{(k)}(\epsilon) \sqrt{\frac{2\epsilon}{m}}\, f(\epsilon, \epsilon_o)\, d\epsilon ,$$

where

$\sigma_i^{(k)}(\epsilon)$ = cross section for electron ionization of i^{th} energy level in k^{th} component as function of electron energy

$\sigma_{ij}^{(k)}(\epsilon)$ = cross section for electron excitation (de-excitation) from i^{th} to j^{th} energy level in k^{th} component as function of electron energy

m = electron mass

$f(\epsilon, \epsilon_o)$ = electron energy distribution function with average energy equal to ϵ_o.

a. Maxwell-Boltzmann Distribution

$$f(\epsilon, \epsilon_o) = \frac{2}{kT_e} \sqrt{\frac{\epsilon}{\pi k T_e}}\, e^{-\epsilon/kT_e}$$

$\epsilon_o = \frac{3}{2} kT_e$

T_e = electron temperatures .

b. Druyvesteyn Distribution

$$f(\epsilon, \epsilon_o) = \frac{2}{\epsilon_o \Gamma(3/4)} \sqrt{\frac{\epsilon}{\epsilon_o}}\, e^{-0.55(\epsilon/\epsilon_o)^2}$$

6. Discharge Resistivity

$$\rho = \frac{3}{2} \frac{m}{e^2 N_e} \sum_k N^{(k)} R^{(k)}$$

$$R^{(k)} = \int_0^\infty \sigma^{(k)}(\epsilon) \sqrt{\frac{2\epsilon}{m}} f(\epsilon, \epsilon_o) d\epsilon \quad ,$$

where:

e = electron charge

$N^{(k)}$ = total number density of k^{th} component

$\sigma^{(k)}(\epsilon)$ = momentum transfer cross section for electron collisions with k^{th} species as function of electron energy.

C. Numerical Procedure and Results

The above system of nonlinear differential equations which results from the model is integrated using the HPCG routine in the Fortran SSP library. The routine was, however, modified so that the step size is controlled by the relative error rather than absolute error. The reason for this is the large dynamic range of the variables involved, as well as their disparate magnitudes. Also, the allowed number of step-size halvings was increased in order to get past the gas-breakdown phase of the time development.

Some preliminary results have been obtained using a prototypic three-level copper energy level structure with no buffer species. These results are reasonable in terms of known experimental behavior, but will not be described, since their only purpose was to aid the program development. It is hoped that this model can be sufficiently well developed so that it will be capable of not only correlating experimental data but also of guiding future experiments in copper, bismuth and other metals.

Joint Services Technical Advisory Committee
F44620-69-C-0047

N. Solimene

REFERENCES

1. W. T. Walter, N. Solimene, J. T. LaTourrette, and K. Park, "Chemically-Generated Copper Vapor Lasers," Progress Report No. 38 to JSTAC, Polytech. Inst. of New York, Report No. R-452.38-73 (1973).

2. K. Park, N. Solimene, and W. T. Walter, "Investigation of Cyclic Laser Action in Bismuth Vapor," Progress Report No. 38 to JSTAC, Polytech. Inst. of New York, Report No. R-452.38-73 (1973).

3. E. T. Gerry, "Pulsed-Molecular-Nitrogen Laser Theory," Appl. Phys. Letters, 7, 6-8 (1965).

4. D. A. Leonard, "A Theoretical Description of the 5106-Å Pulsed Copper Vapor Laser," IEEE J. Quantum Electron., QE-3, 380-81 (1967).

5. M. Gryzinski, "Classical Theory of Atomic Collisions. I. Theory of Inelastic Collisions," Phys. Rev., 138A, 336-58 (1965); also, A. E. S. Green, "Electron Impact Cross Sections for Aeronomy," AIAA J., 4, 769-75 (1966).

APPENDIX III

STRATIFIED WAKES

The work on the subject of wake behavior in stratified flows was carried out in prior contract periods (DARPA-STO program administered by the U.S. Army Research Office under contract DAHCO4-69-C-007) . However, the reports were completed under the current contract and will be issued under its auspices.

One report by G.H. Strom[1] presents an account of the final development of the Polytechnic's thermally-stratified air wind-tunnel, its calibration and operation. It also presents experimental results of a series of experiments on wakes in this stratified flow under conditions intended to simulate wakes in ocean thermoclines, and related modeling criteria. This work is believed to be a milestone achievement in stratified flow simulation.

A second report by P. Khosla[2], presents a preliminary study of the theoretical treatment of a shear flow in the form of a jet within a thermally stratified flow. It depicts some of the difficulties involved in formulating a formally correct theory, and points the way to further work which may lead to satisfactory solutions.

REFERENCES

1. Strom, Gordon H.: "Wind Tunnel Experiments on Wakes in Stratified Flow Including Modeling Criteria and Development of Experimental Equipment" POLY-AE/AM Report 76-11, June 1976.

2. Khosla, P. : Internal Memo, "On The Theory of Jets in Stratified Flow" POLY-AM Memo 75-01, June 1975.